



IAHR Ice Symposium 1986
Iowa City, Iowa

AN INTEGRATED CONSTITUTIVE THEORY FOR THE MECHANICAL
BEHAVIOR OF SEA ICE: EXPERIMENTAL VERIFICATION

S. Shyam Sunder
Winslow Associate
Professor of Civil
Engineering

Massachusetts Institute
of Technology

Cambridge
MA, USA

Abstract

A rate-sensitive constitutive theory is developed for describing the mechanical behavior of sea ice. The theory is characterized by its ability to:

- (a) Decompose the various recoverable (instantaneous elastic and delayed elastic or primary creep) and irrecoverable (secondary creep and strain-softening or tertiary creep) components of strain.
- (b) Describe materially anisotropic material behavior with a pressure-insensitive but rate-dependent potential function.
- (c) Represent continuously damaging or strain-softening material behavior during ductile-to-brittle transition in compression with a linear incremental damage accumulation model.
- (d) Predict first crack occurrence or nucleation with a rate-dependent limiting tensile strain criterion.
- (e) Describe ultimate failure by macrocracking representing either yielding of the material or fracture with a rate and pressure sensitive Drucker-Prager surface.

This paper compares the model predictions with several independent sets of experimental data, particularly those for first-year sea ice. Data for the uniaxial "strength" of sea ice is augmented with the extensive experimental data base available for pure polycrystalline ice through a normalization to account for the presence of brine.

Theoretical Formulation

Continuum Theory.-- The constitutive model is a nonlinear generalization of the two element Maxwell fluid model consisting of a rate-sensitive spring with effective modulus, E_{eff} , connected in series to a nonlinear viscous dashpot. The governing equations are listed in Table 1.

The effective modulus equals the Young's modulus, E , at very high rates of loading and $(1-r)E$ as the strainrate approaches zero, where r is a parameter that models stress relaxation. If $r=1$ the material displays no stress relaxation and if $r=0$ the effective modulus is rate-insensitive and equal to the Young's modulus. Typically, r is less than one. The effective modulus represents the recoverable strains contributed both by instantaneous elasticity and by delayed elasticity. As such, the rate-sensitive spring can be decomposed into two springs in series, one with modulus equal to E , the Young's modulus, and another with modulus equal to E_d , the modulus of delayed elasticity.

The nonlinear viscous dashpot represents the secondary creep strainrate based on the well known Glen's power law. Note that the parameter A controls secondary creep as well as delayed elasticity.

Material damage or microcracking activity in ice leads to tertiary creep under constant stress loading and to strain-softening under constant strainrate loading. The phenomenon affects both the rate-sensitive spring and the nonlinear dashpot which governs ice behavior at larger strains. The development here is based on the hypothesis that damage influences the constant A describing the creep resistance of ice. The effect of damage on the Young's modulus is neglected. Defining D as a one-dimensional damage parameter, it is possible to express the damaged value of the creep resistance parameter A as $A_D=(1-D)A$. In general, D varies between zero and one; it equals zero in the case of no damage and one for total damage, i.e., the material loses all ability to sustain stresses. The mathematical formulation of damage in Table 1 is appropriate for monotonic loading conditions. For a variable loading

history, the evolution of damage is assumed to follow the well-known Miner's linear damage accumulation rule.

The effect of temperature on the creep resistance of ice, i.e., the parameter A , is modelled in terms of the Arrhenius activation energy law which is valid for ice below -10°C . The use of this law for both delayed elasticity and secondary creep has been previously justified by Sinha (1978). Both the Young's modulus of ice and the microcracking activity in ice is taken to be insensitive to temperature variations.

The multiaxial generalization of the nonlinear deformations in sea ice is based on a flow potential, not a yield surface. This description allows recoverable and irrecoverable deformations to occur simultaneously in accordance with the generalized Maxwell model for uniaxial deformations. The material anisotropy in ice is formulated in terms of an orthotropic model. The instantaneous elastic strains follow the classical orthotropic models of elasticity theory, while the creep strains follow a generalized pressure insensitive flow potential in stress space (the flow potential resembles that corresponding to the von-Mises yield surface of plasticity theory when generalized for material anisotropy). The five flow potential constants defining material anisotropy are identified in Table 1. They can be derived from conventional uniaxial tests conducted in five directions oriented in and at a 45° angle to the axes of orthotropy. The sixth (reference) direction provides the uniaxial model parameters.

Yielding and Fracture Theory.-- The theory for the yielding and fracture of ice is based on three principal behavioral regimes: (a) for strainrates below a transition strainrate, e.g., $5 \times 10^{-8} \text{ s}^{-1}$, ice behaves essentially as a continuum (flowing material) in both compression and tension, (b) for strainrates greater than a transition strainrate, e.g., 10^{-2} s^{-1} , the strength of ice is governed by brittle failure in both compression and tension, and (c) at intermediate strainrates ice behaves as a damaging continuum in compression and as a fracturing material in tension (for the range of grain sizes typically encountered in sea ice).

The tensile "fracture" strength σ_{tf} of typical sea ice is governed by the stress to nucleate a crack. The variation of this strength with strainrate is modelled by the expression listed in Table 1. The ductile-to-brittle transition in tension tends to occur over a negligible range of strainrates.

In compression, the "strength" at intermediate strainrates is governed by the stress to propagate cracks. This is the maximum stress predicted by the continuum model. The stress at which the first "important" microcrack, i.e., one that is visible to the naked eye in pristine ice, nucleates is defined as the "yield" stress σ_{cn} . Prediction of first crack nucleation is based on the hypothesis that this occurs due to the lateral tensile strain and strainrate resulting from the Poisson effect of elasticity and the incompressibility condition of creep deformation. The first crack is postulated to occur when the lateral tensile strain equals the strain for fracture under uniaxial tensile loading at the instantaneous strainrate. The strain for tensile fracture at a given strainrate can be obtained from tensile stress-strain-strainrate-strength model. This results in a rate dependent limiting tensile strain criterion for first crack occurrence or nucleation. Following this approach, the variation of compressive yield stress with strainrate can be determined as shown in Table 1. At high strainrates, the yield stress and the compressive strength become equal.

A rate-sensitive and isotropic Drucker-Prager "failure" surface is used to describe the yield and fracture behavior of ice. Thus, the model developed here considers the failure surface to be pressure sensitive although the flow behavior is pressure insensitive. At any given strainrate, the two constants of the Drucker-Prager model are obtained from two uniaxial tests, one in compression and the other in tension. Making use of the models for strainrate variation of the tensile fracture strength and the compressive yield stress, explicit equations can be derived for the rate-sensitive description of the two constants. The multiaxial generalization is based on an effective strainrate definition. Experimental data is not available at the present time to model anisotropy in the yield and fracture behavior.

The flow surface describing the continuum deformation of ice and the Drucker-Prager surface describing yielding and fracture will in general intersect. Under all states of stress which involve at least one tensile stress, the Drucker-Prager surface will define the limiting surface that the material can attain prior to fracture. The direction of cracking is assumed to be perpendicular to the largest principal tensile stress. When no tensile stress exists, the Drucker-Prager surface defines yield, but stress states can attain the limiting flow surface associated with the continuum deformation. If the yield surface is intersected, a crack nucleates in the direction of the smallest compressive stress and the material loses its ability to sustain a tensile stress in that direction if applied at a later time.

Experimental Verification

Extensive verification of the model has been carried out using experimental data on pure as well as sea ice. Since sea ice is a porous material consisting of brine pockets, an effective stress can be defined for the stress transmitted by the solid ice using the brine volume normalization proposed by Weeks and Assur (1967). In turn, the brine volume can be related to the temperature and salinity of ice through the relationship proposed by Frankenstein and Garner (1967). Use of the effective stress measure provides a unifying basis for comparing pure and sea ice data.

Constant Strainrate Tests.-- The maximum stress (termed "strength" for convenience) observed from constant strainrate tests in compression is plotted against strainrate in Fig. 1 after brine volume normalization. The solid line in the figure represents the prediction of the rate-sensitive damage model proposed here; the model captures the trend of the data very well. For strainrates greater than 10^{-2} s^{-1} the continuum model of damage is invalid and a horizontal line representing fracture is drawn at a stress of 5.0 MPa. The dashed line in the figure is the familiar power law model for secondary creep which fails to model

material damage resulting in strain-softening for strainrates between 10^{-4} s^{-1} and 10^{-2} s^{-1} . The maximum value of strength increases by about 42% from about 10 MPa to 14.2 MPa as temperature is reduced from -10°C to -20°C .

Typical stress-strain curves predicted by the model are shown in Fig. 1. The lowering of residual stress at higher strainrates as a result of strain-softening, observed for example by Wang (1982), is correctly predicted by the model.

Creep Tests.-- Experimental limitations preclude the possibility of conducting an ideal creep test. In most cases a finite period of time equivalent to a few seconds is necessary to develop the nominal creep stress. This finite rise time governs the extent of primary creep deformation for the proposed model. Prediction of creep curves based on a postulated exponential time variation of the applied stress is able to describe experimental data as well if not better than the model of Sihna (1978). A typical model prediction is shown in Fig. 2.

Constant Stressrate Tests.-- The limited experimental data from constant stressrate tests is plotted in Fig. 3. For stressrates greater than about 0.05 MPa s^{-1} , the fracture strainrate of 10^{-2} s^{-1} is reached only after the stress exceeds 5 MPa, the fracture stress at this strainrate in constant strainrate tests. Assuming that in constant stressrate tests material failure is governed by the fracture strainrate, not fracture stress, the maximum stress just prior to fracture defines the strength. The validity of this assumption is justified since the model predicts the observed behavior quite well. For lower stressrates, the model overpredicts the strength. A careful study of the complete stress-strain curves shows that experimental observations are made prematurely and do not represent the actual "strength" value. If the stress at 1% strain, i.e., the strain at which Wang (1982) made his observations, represents the prediction, Fig. 3 shows that the model captures the overall data trend very well.

Effective Elastic Modulus.-- Figure 4 shows the predicted and observed strainrate variation of the effective elastic modulus for ice. The figure indicates an excellent match with the relaxation parameter $r=0.51$.

Multiaxial Flow Behavior.-- The pressure insensitive but rate dependent material model for the multiaxial flow behavior of ice follows very well the experimental data of Frederking (1977) on the plane strain compressive strength of columnar grained and granular-snow ice. Verification of the model against data on sea ice (Fig. 5), which is significantly less pressure sensitive than pure ice (see Richter-Menge et al., 1985, for data on anisotropic first year sea ice), suggests that a pressure insensitive model may be adequate in many engineering applications. This is particularly true when considering the large spread in the uniaxial experimental data (Fig. 1). It must be noted that the plasticity based pressure sensitive parabolic yield function of Reinicke and Ralston (1977) has been justified with the help of Frederking's (1977) data (which has been shown to follow the pressure insensitive model proposed here very well) and that the three parameter extension of their yield function by Reinicke and Remer (1978) has been justified on the basis of triaxial data for pure polycrystalline ice.

Prediction of First-Crack Occurrence.-- Figure 6 contains the prediction of first crack occurrence or nucleation during compressive creep tests using the limiting tensile strain criterion for yield/fracture. Comparison with the experimental data of Gold (1972) shows that, once again, the proposed model captures the overall trend of the data very well. In particular, the time to first crack asymptotically approaches infinity as the compressive stress reduces to 0.48 MPa. The choice of stress-strainrate at which ice transits from ductile to fracture behavior in tension, i.e., 0.48 MPa and $5 \times 10^{-8} \text{ s}^{-1}$, determines this asymptote. Data scatter may be due to several reasons, including model uncertainty. However, two sources stand out; first, the finite rise time required for the applied stress to reach the nominal creep stress, and second, uncertainties associated with the identification/definition

of the "first" crack during testing. The limiting tensile strain criterion compares well with the delayed elastic strain criterion for crack nucleation proposed by Sinha (1982).

Multiaxial Yield/Fracture Behavior.-- The intersection of the yield/-fracture surface with the limiting flow surface for continuum response under plane stress conditions is shown in Fig. 7 at an effective strain-rate of 10^{-5} s^{-1} . Comparison of the model prediction with the triaxial data of Haynes (1973) on bubbly polycrystalline ice in the tension-compression quadrant shows an excellent match; in particular, the ratio of the uniaxial compressive yield stress to the uniaxial tensile fracture strength approaches approximately 1.7 for both the model and the test data. None of the classical biaxial failure envelopes for brittle materials that Haynes considered explained the data as well.

Conclusions

This paper has presented a new and integrated constitutive theory for the continuum and yielding/fracture behavior of sea ice. The model has been extensively verified against experimental data. A research report written by Ting and Shyam Sunder (1985) describes the model development in detail.

Current research by the author's research group is concerned with the development of (a) an objective energy release rate criterion for modifying the "strength" based fracture criterion, (b) an anisotropic and pressure sensitive model for material damage resulting from microcracking, (c) a predictive model for the influence of brine volume, or more generally porosity, on the multiaxial behavior of ice, and (d) an improved yield/fracture surface for large values of (compressive) hydrostatic stress.

Acknowledgements

The author would like to thank his graduate students, particularly Dr. Seng-Kiong Ting (now on the faculty of the National University of

Singapore), who have actively participated in this research. The support and encouragement of Professors Jerome J. Connor and Charles C. Ladd is gratefully acknowledged. This research is funded by The Standard Oil Company through MIT's Center for Scientific Excellence in Offshore Engineering, and cosponsored by the U.S. Department of the Interior, Minerals Management Service.

References

- Frankenstein, G. and Garner, R., 1967. Equations for Determining the Brine Volume of Sea Ice from -0.5° to -22.9°C . *Journal of Glaciology*, 6(48), p.943-944.
- Frederking, R., 1977. Plane Strain Compressive Strength of Columnar-Grained and Granular-Snow Ice. *Journal of Glaciology*, 18(80), p.505-516.
- Gold, L.W., 1972. The Process of Failure of Columnar-Grained Ice. *Philosophical Magazine*, 26(2), p.311-328.
- Haynes, F.D., 1973. Tensile Strength of Ice Under Triaxial Stresses. USA CRREL Research Report 312, U.S. Army Cold Regions Research and Engineering Laboratory, Hanover, NH, 21p.
- Reinicke, K.M. and Ralston, T.D., 1977. Plastic Limit Analysis with an Anisotropic, Parabolic Yield Function. *International Journal of Rock Mechanics, Mining Sciences and Geomechanics*, 14, p.147-154.
- Reinicke, K.M. and Remer, R., 1978. A Procedure for the Determination of Ice Forces - Illustrated for Polycrystalline Ice. *Proceedings of the IAHR Ice Symposium, Lulea, Sweden*, p.217-238.
- Sinha, N.K., 1978. Rheology of Columnar-Grained Ice. *Experimental Mechanics*, 18(12), p.464-470.
- Sinha, N.K., 1982. Delayed Elastic Strain Criterion for First Cracks in Ice. *Proceedings of the IUTAM Symposium on Deformation and Failure of Granular Materials, Delft, The Netherlands*, p.323-330.
- Ting, S-K. and Shyam Sunder, S., 1985. Constitutive Modeling of Sea Ice with Applications to Indentation Problems. CSEOE Report No. 3, Massachusetts Institute of Technology, Center for Scientific Excellence in Offshore Engineering, Departments of Civil Engineering and Ocean Engineering, 255p.
- Wang, Y.S., 1982. A Rate-Dependent Stress-Strain Relationship for Sea Ice. *Proceedings of the First International Symposium on Offshore Mechanics and Arctic Engineering, New Orleans, LA*, p.243-248.
- Weeks, W. and Assur, A., 1967. The Mechanical Properties of Ice. USA CRREL Report II-C3, U.S. Army Cold Regions Research and Engineering Laboratory, Hanover, NH.

Table 1 Governing Equations for Constitutive Theory

Maxwell Fluid Model

$$\text{Effective Elastic Modulus: } E_{\text{eff}} = E [1 - r \exp(-A/E \dot{\epsilon}^{1/N})]$$

$$\text{Nonlinear Viscous Dashpot: } \sigma = (A/M) \dot{\epsilon}_{\text{sc}}^{1/N}$$

Material Damage

$$D = 1 - [\exp(-c_1 \dot{\epsilon}) + \exp(-c_2 \dot{\epsilon}) \{1 - \exp(-c_1 \dot{\epsilon})\}]$$

Temperature Effect

$$A = A_0 \exp(Q/NRT)$$

Effective Stress for Multiaxial Flow Potential

$$\sigma_e^2 = 3/(a_1 + a_2) \left[\frac{a_1}{3} (\sigma_{xx} - \sigma_{yy})^2 + \frac{a_2}{3} (\sigma_{yy} - \sigma_{zz})^2 + \frac{a_3}{3} (\sigma_{zz} - \sigma_{xx})^2 \right. \\ \left. + 2a_4 \sigma_{xy}^2 + 2a_5 \sigma_{yz}^2 + 2a_6 \sigma_{zx}^2 \right]$$

with $a_1=1$ without loss of generality

Tensile Fracture Strength

$$\frac{1}{\sigma_{\text{tf}}} = \frac{1}{\sigma_{\text{tm}}} + \frac{1}{B \dot{\epsilon}^{1/N}}$$

Compressive Yield Strength

$$\frac{1}{\sigma_{\text{cn}}^2} = \frac{1}{\sigma_{\text{cm}}^2} + \frac{1}{[(A/M) \dot{\epsilon}^{1/N}]^2}$$

Drucker-Prager Surface for Yield/Fracture

$$f(\sigma) = p I_1 + \sqrt{J_2} - k$$

with I_1 = first invariant of stress vector
 J_2 = second invariant of deviatoric stress vector

$$p = \frac{1 (\sigma_{\text{cn}}/\sigma_{\text{tf}}) + 1}{3 (\sigma_{\text{cn}}/\sigma_{\text{tf}}) - 1} \quad \text{and} \quad k = \sigma_{\text{cn}} (p - 1/\sqrt{3}) \text{ or } \sigma_{\text{tf}} (p + 1/\sqrt{3})$$

Material Constants

$E=9.5$ GPa, $r=0.98$, $A_c=9.201$ MPa $\text{s}^{1/N}$, $N=3$, $M=1411.2$, $Q=65$ kJ mol^{-1}
 $c_1=2.28 \times 10^5$ s, $c_2=1028$ s, $R=8.314$ J mol^{-1} K^{-1} , $\sigma_{\text{tm}}=2.0$ MPa,
 $B=176$ MPa $\text{s}^{1/N}$, $\sigma_{\text{cm}}=5.0$ MPa, and a_2 - a_6 depend on the anisotropy.

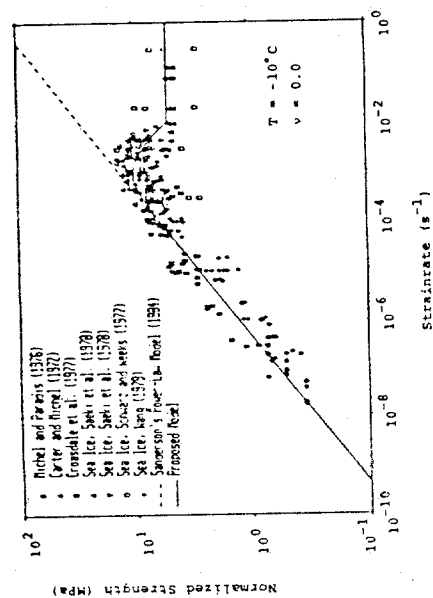


Figure 1a

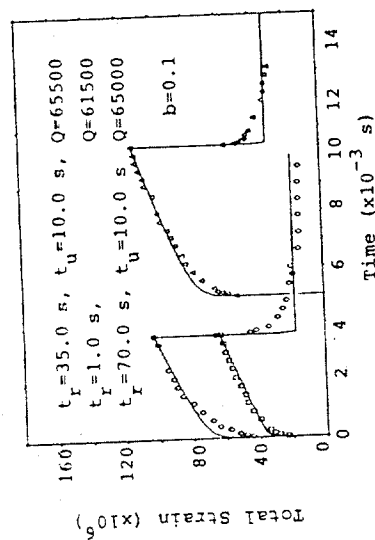


Figure 2

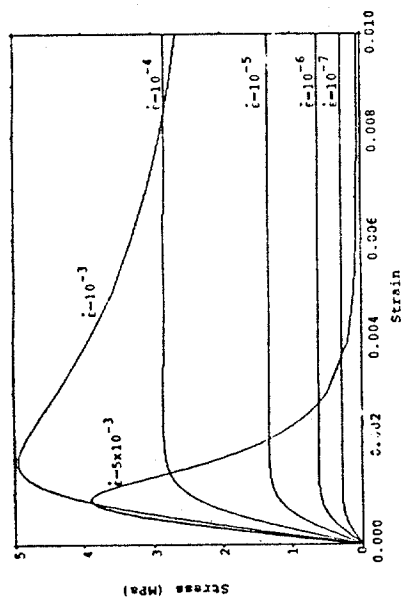


Figure 1b

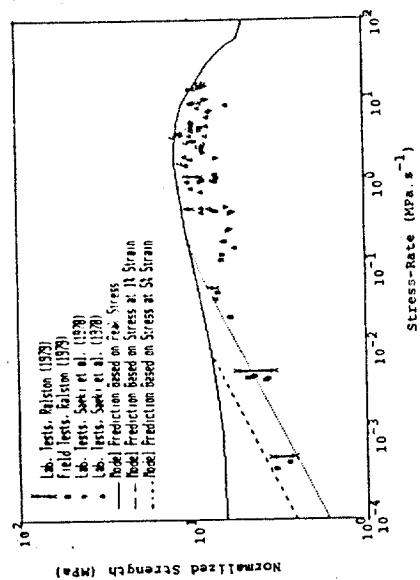


Figure 3

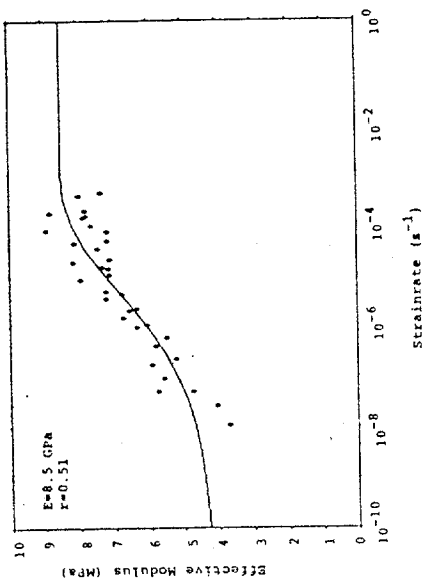


Figure 4

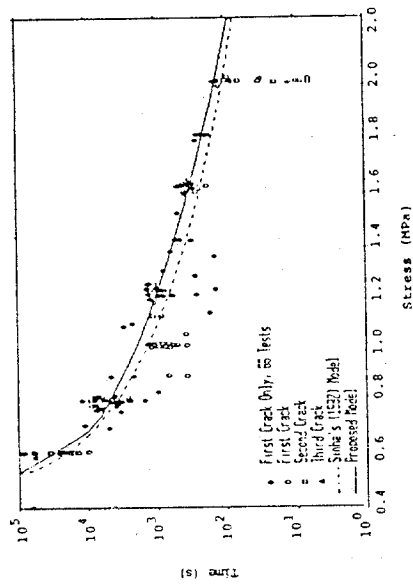


Figure 6

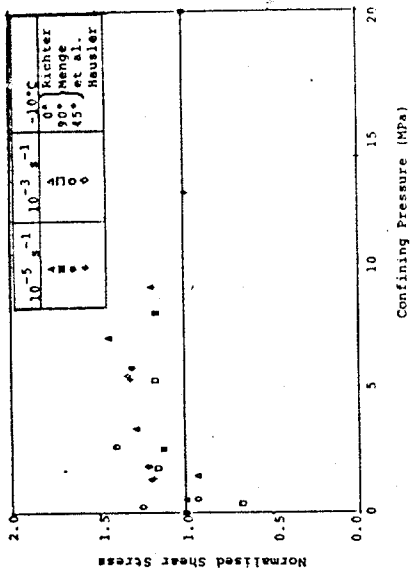


Figure 5

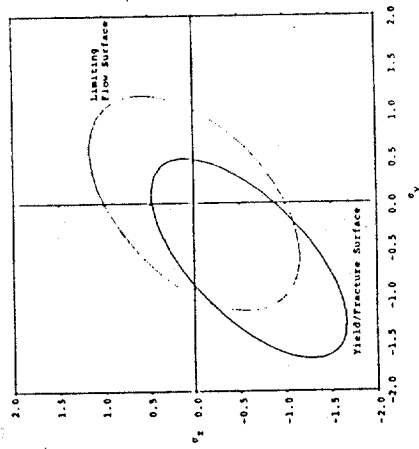


Figure 7